Electronic Supporting Information

Charge Transfer Aided Selective Sensing and Capture of Picric Acid by Triphenylbenzenes

Pratap Vishnoi, Saumik Sen, G. Naresh Patwari,* and Ramaswamy Murugavel*

Department of Chemistry,
Indian Institute of Technology Bombay, Mumbai, India-400 076

G. Naresh Patwari

E-mail; naresh@chem.iitb.ac.in,

Ramaswamy Murugavel

rmv@chem.iitb.ac.in

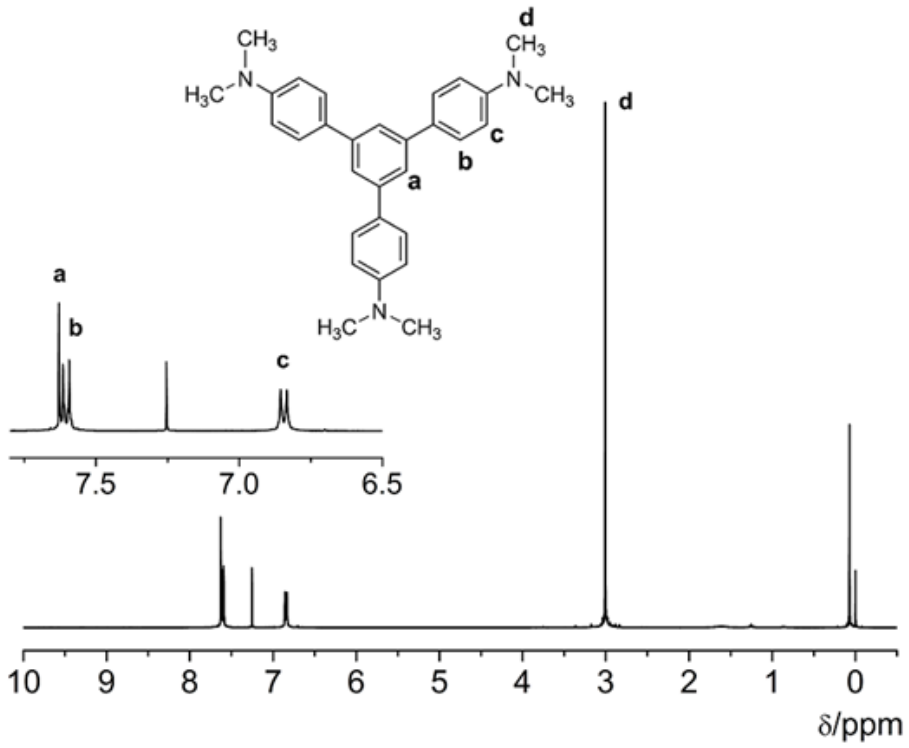

Fig S1. ^{1}H NMR spectrum of [(*N*,*N*)Me$_2$]$_3$-TAPB in CDCl$_3$.

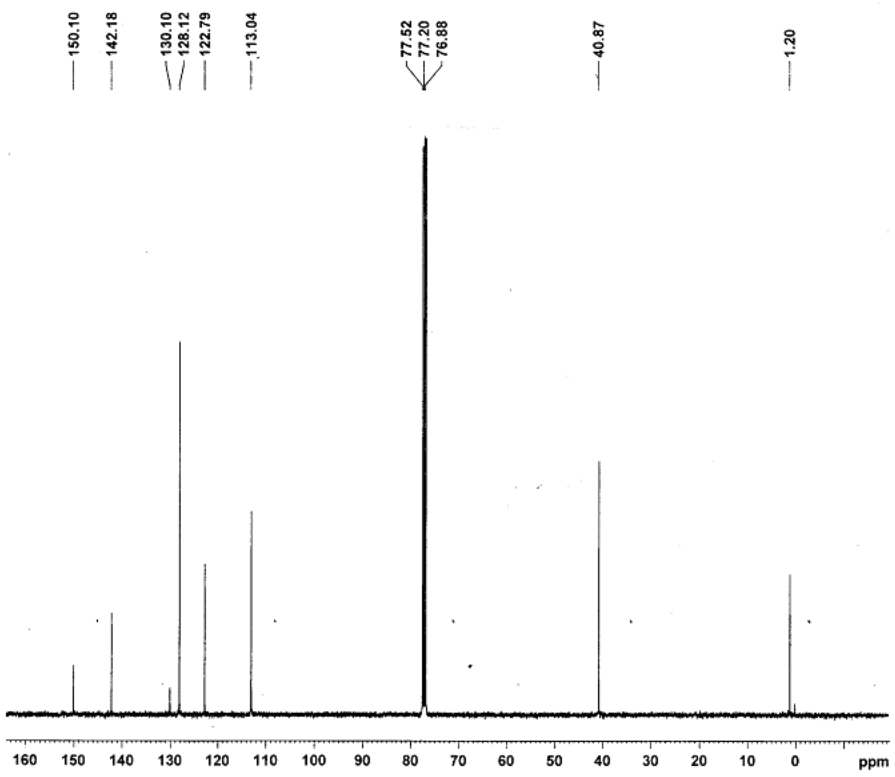

Fig S2. ^{13}C NMR spectrum of [(*N*,*N*)Me$_2$]$_3$-TAPB in CDCl$_3$.

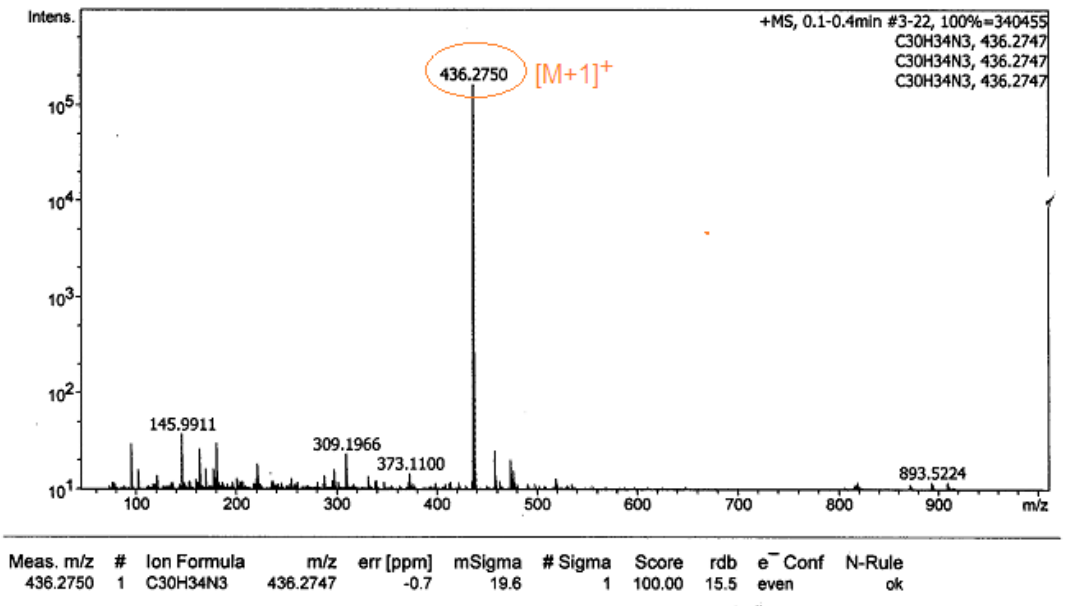

Fig S3. ESI-MS spectrum of $[(N,N)Me_2]_3$-TAPB.

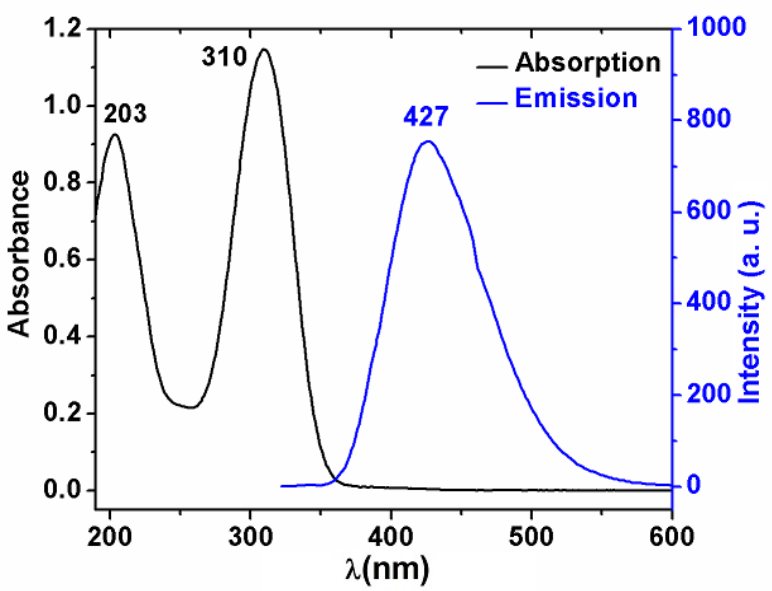

Fig S4. UV-Vis absorption spectrum (10 μM; λ_{max} = 203 nm (ε = 8 × 10^4 $M^{-1}cm^{-1}$); λ_{max} = 310 nm (ε = 1.1 × 10^5 $M^{-1}cm^{-1}$) and emission spectrum (1.0 μM, λ_{ex} = 310 nm and λ_{em} = 425 nm) of $[(N,N)Me_2]_3$-TAPB.

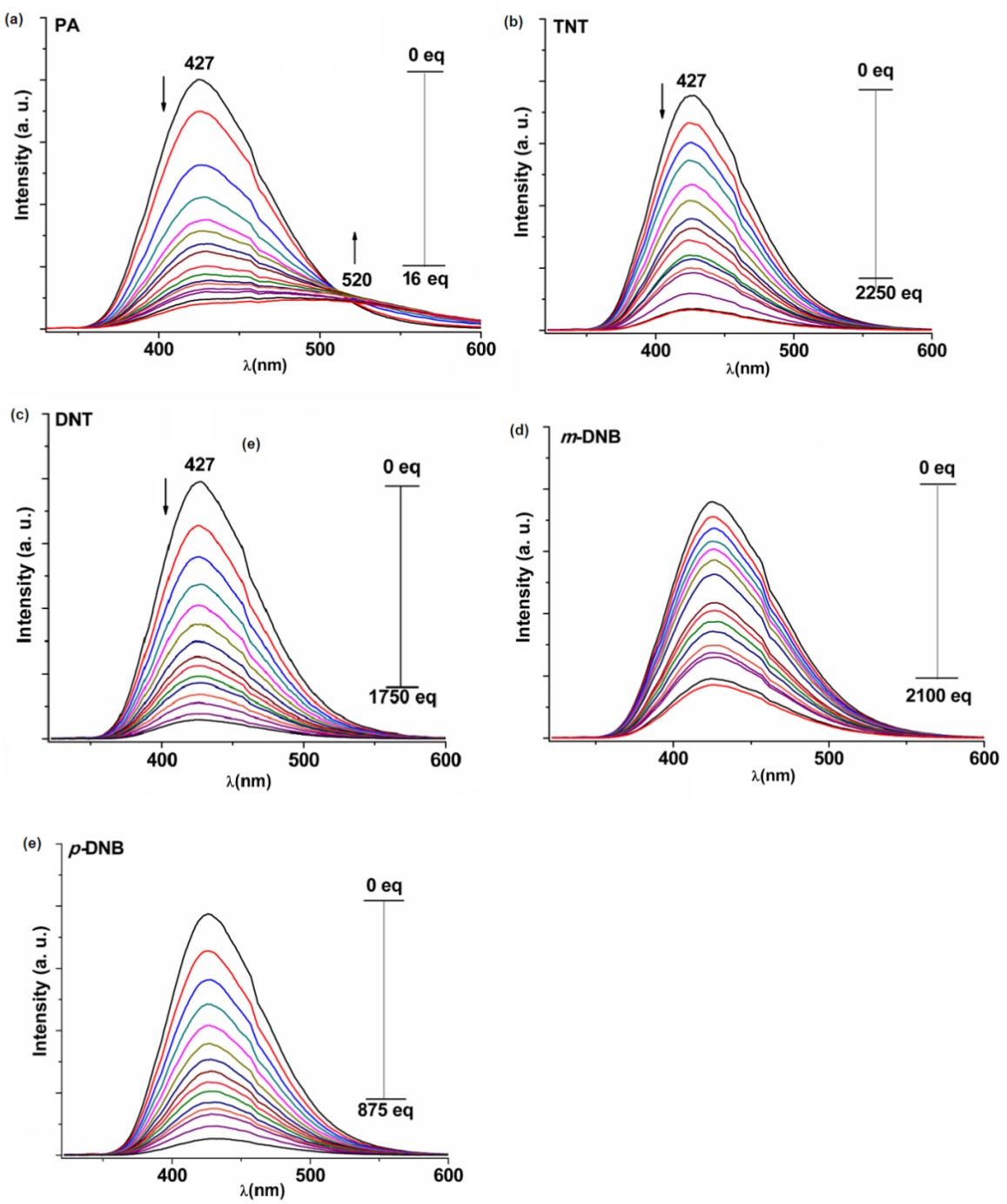

Fig S5. Fluorescence quenching profiles of [(*N*,*N*)Me_2]$_3$-TAPB in acetonitrile (1.0 μM) with various concentrations of PNAC analytes, (a) with PA, (b) with TNT, (c) with DNT, (d) with *m*-DNB and (e) with *p*-DNB.

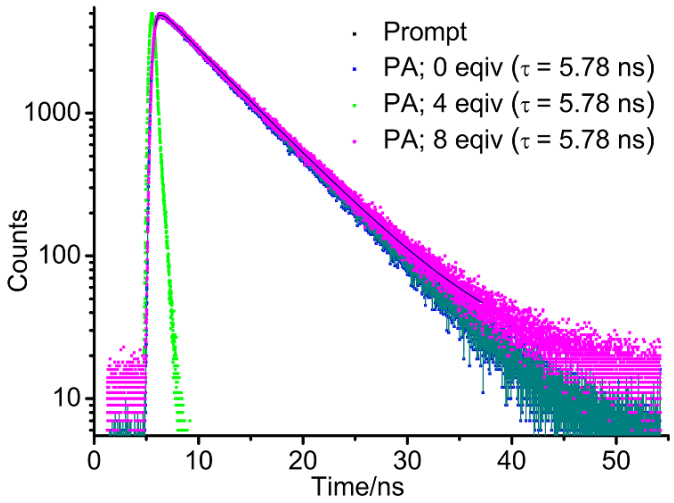

Fig S6. Time resolved fluorescence decays for an acetonitrile solution of [(*N*,*N*)Me_2]$_3$-TAPB before and after multiple additions of known concentrations of PA.

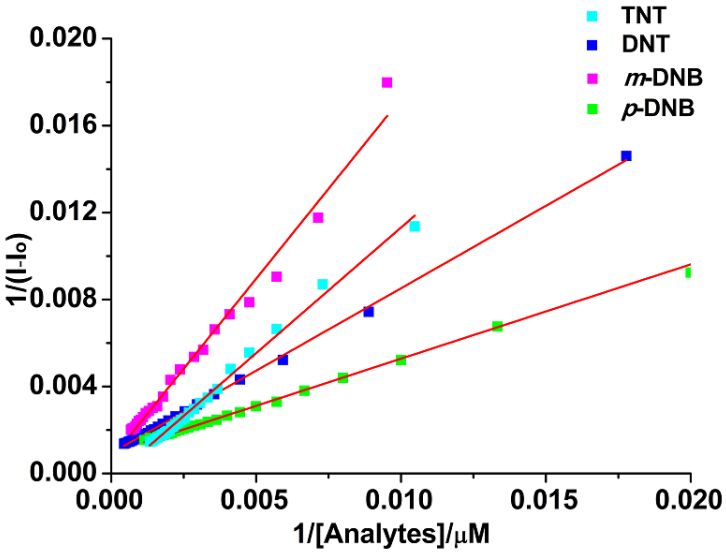

Fig S7. Benesi-Hildebrand plots of [(*N*,*N*)Me_2]$_3$TAPB with TNT, DNT, *m*-DNB and *p*-DNB.

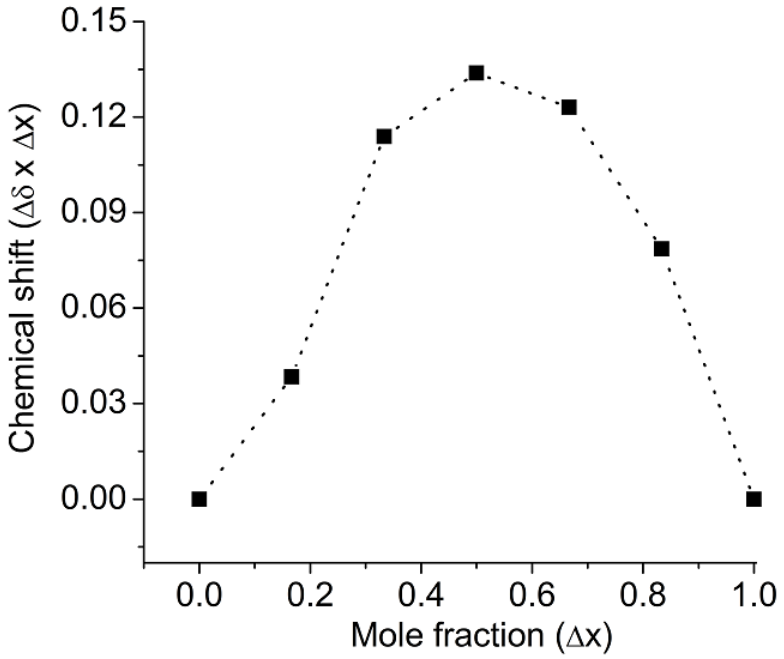

Fig S8. Job's plot of [(*N*,*N*)Me_2]$_3$TAPB with PA showing complexation in 1:1 stoichiometry.

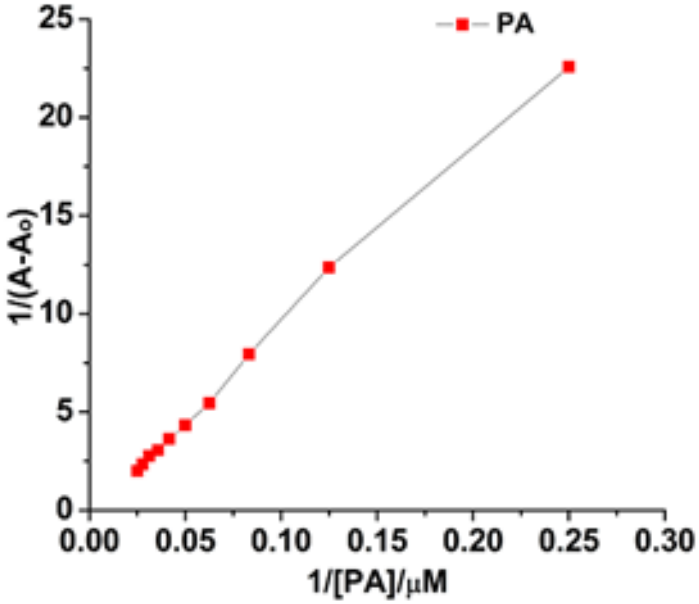

Fig S9. Benesi-Hildebrand plots of [(*N*,*N*)Me_2]$_3$-TAPB with PA obtained from UV-Vis absorption titration.

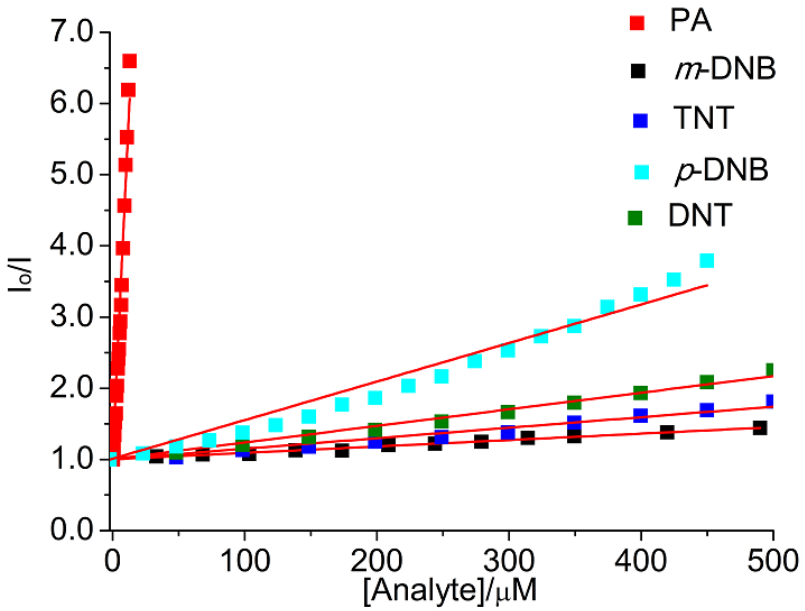

Fig S10. The Stern-Volmer plots of $[(N,N)Me_2]_3$TAPB obtained from fluorescence quenching titration of different PNAC analytes (PA, TNT, DNT, *m*-DNB and *p*-DNB).

Table S1. Details of quenching efficiencies for $[(N,N)Me_2]_3$-TAPB with various concentrations of different PNAC analytes.

Analyte(s)	Equivalent(s) added	% Quenching	K_{sv} (M^{-1})
PA	8	75	3.31×10^5
TNT	2250	90	1.90×10^3
m-DNB	2100	77	3.03×10^3
DNT	1720	92	1.23×10^3
p-DNB	875	93	5.44×10^3

Table S2. Comparison of present results with previously reported PA sensors.

Chemo-sensor	K_{sv} (M^{-1})	Detection Limit	Analyte	Solvent	Ref
hexaphenylsilole	-	4.81 ppb	Only PA	THF/water or water	1
tetraphenylethene	2.7×10^5	0.4 ppm	Only PA	water	2
trigonal-prismatic Ru(III) cages	PA; 1.0×10^5 TNT; 2.1×10^4	-	PA = 45.8 μM TNT = 148.9 μM (70 % quenching)	methanol	3
poly(silylenevinylene)	8.491×10^3 M^{-1} in THF 6.36×10^4 M^{-1} in water	~ 1.0 ppm	94.3 mM in THF; 21.5 mM in THF/water	THF/water	4
terthiophene	5.7×10^3	70 ppb	PA, TNT, DNT and NB	Water	5
pentacenequinone	PA; 6.9×10^4 TNT; 4.3×10^3	500 ppb	PA, TNT, DNT and *p*-DNB;	THF/water	6
p-phenylenevinylene	5.51×10^4	2.71 ppb	PA TNT, DNT, NB, DNB, DNP, selective to PA and DNP	water	7
fluoranthene	9.9×10^4	2-200 ppb	only PA	Ethanol	8
tetraphenylethylene	5.7×10^4	1.45 ppb	Selective to PA against TNT and DNT	THF/water	9
amphiphilic cellulose	PA; 1.486×10^3 (in THF) & 1.02×10^5 (in H_2O) DNT; 2.21×10^2 (in THF) 1.1 1 x 10^4 (in H_2O)	-	PA and DNT	THF or water	10
hexa-peri-hexabenzocoronene	3.2×10^6 & 2.9×10^6	0.9 ppb & 1.9 ppb	PA, DNB, TNT, DNT, *p*-NT, NB	THF/water	11
N-acylhydrazone derivatives	4.93×10^5, 3.85×10^5, 5.12×10^5 , 3.02×10^5	-	PA	DMF	12
azine based covalent organic framework	7.8×10^5	-	PA, TNT and DNT	Acetonitrile	13
hexaphenylbenzene	1.95×10^5	6.87 ppb	PA, TNT, DNT and DNB	THF/water	14
triaminophenylbenzene	1.2×10^5	-	PA, TNT, DNT, *m*-DNB and *p*-DNB	Acetonitrile	15
tris-dimethylaminophenylbenzene	3.87×10^5	1.50 ppm	PA, TNT, DNT, *m*-DNB and *p*-DNB	Acetonitrile/water	this work

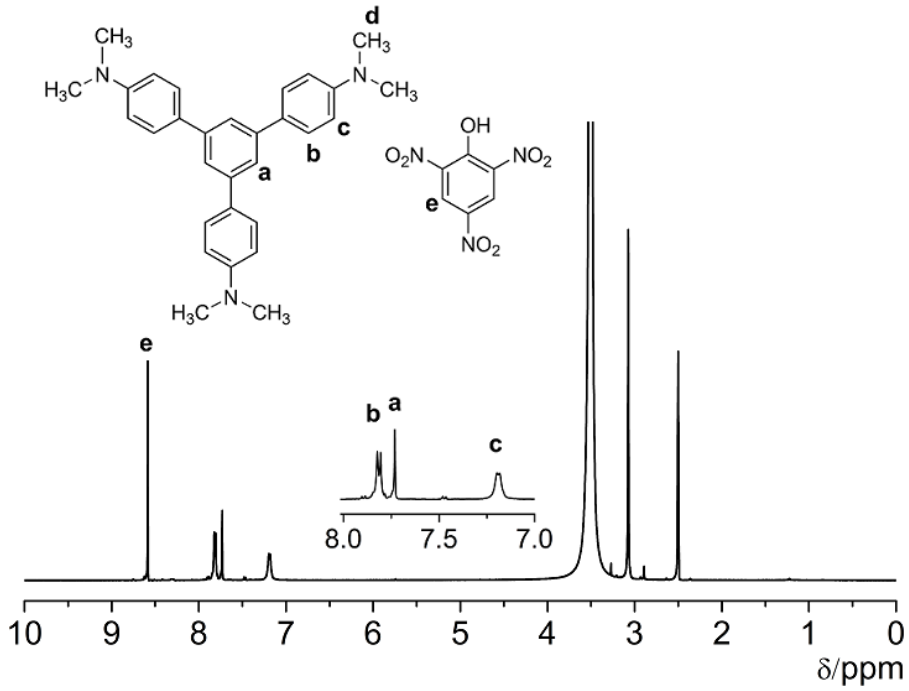

Fig S11. ^{1}H NMR spectrum of [(*N*,*N*)Me$_2$]$_3$-TAPB-PA in DMSO-d_6.

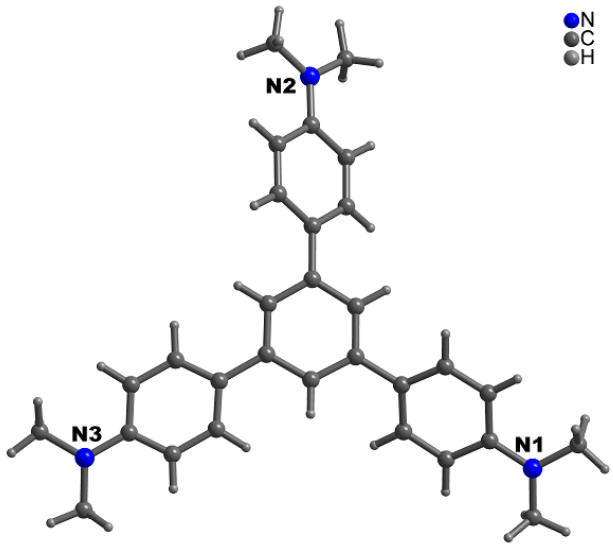

Fig S12. X-ray crystal structure of [(*N*,*N*)Me$_2$]$_3$-TAPB.

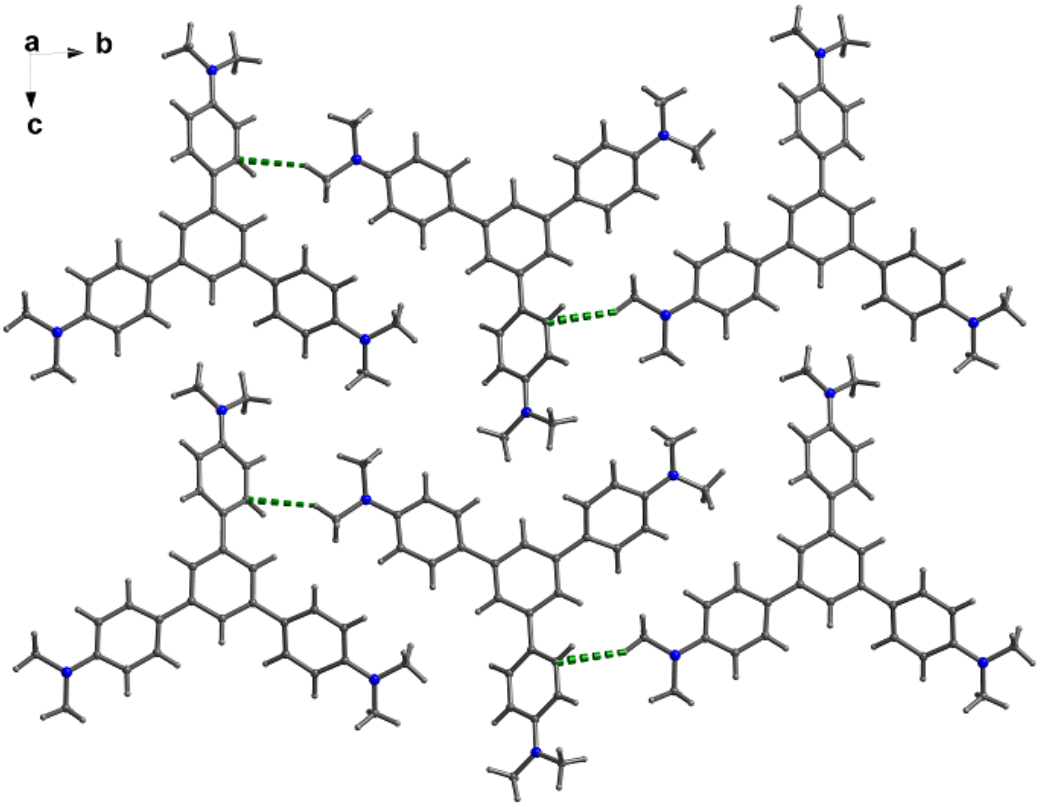

Fig S13. A view of a 1-D layer of the crystal structure of [(*N*,*N*)Me_2]$_3$-TAPB along the crystallographic direction *a* (H-bonds are shown by green dashed bonds).

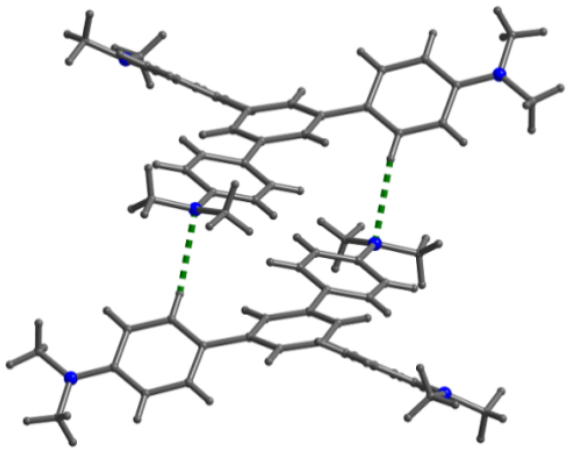

Fig S14. Crystal structure of [(*N*,*N*)Me_2]$_3$TAPB showing mutual C-H···N interactions between two molecules present in the adjacent layers (H-bonds are shown by green dashed bonds).

Table S3. Crystal data and structure refinement details for[(N,N)Me_2]$_3$TAPBand[(*N*,*N*)Me_2]$_3$TAPB-PA.

Compound(s)	**[(N,N)Me_2]$_3$TAPB**	**[(*N*,*N*)Me_2]$_3$TAPB-PA**
formula	$C_{30}H_{33}N_3$	$C_{48}H_{42}N_{12}O_{21}$
formula wt	435.59	1122.94
temperature [K]	150(2)	150(2)
wavelength [Å]	0.71075	0.71075
crystal system	monoclinic	triclinic
space group	$P2_1/c$	P-1
a [Å]	13.508(9)	10.766(3)
b [Å]	24.193(16)	13.960(5)
c [Å]	7.507(5)	17.294(6)
α [deg]	90	102.357(5)
β [deg]	94.8640(10)	98.189(5)
γ [deg]	90	100.935(4)
volume (Å)^3	2444(3)	2447.0(14)
Z	4	2
density (calcd) [g/cm^3]	1.184	1.524
absorption coeff (mm^{-1})	0.069	0.122
F(000)	936	1164
crystal size [mm^3]	0.02 × 0.05 × 0.25	0.02× 0.06 × 0.14
θ range [deg]	2.85 to 25.00	2.52-25.00
reflection collected	18213	18789
data (Rint)	4282(0.0722)	8546(0.0354)
completeness to θ [%]	99.7	99.1
restraints/parameters	36/329	0/730
GoF on F^2	1.303	1.087
R1 [I>2σ(I)]/all data	0.1283/0.1581	0.0662/0.0852
wR2 [I>2σ(I)]/all data	0.2274/0.2450	0.1486/0.1486
Largest peak and hole (e, Å-3)	0.297, -0.229	0.331, -0.264

Table S4. Geometrical parameters for hydrogen bonds (distances in Å and angles in deg) of [(*N*,*N*)Me$_2$]$_3$TAPB and [(*N*,*N*)Me$_2$]$_3$TAPB-PA.

Compound(s)	D-H···A	d(D-H)	d(H···A)	d(D···A)	<(DHA)
[(*N*,*N*)Me$_2$]$_3$TAPB	C(8)-H(8)···N(3)	0.95	2.66	3.524(5)	151
	C(29)-H(29A)···C(16)	0.98	2.89	3.777(3)	151
[(*N*,*N*)Me$_2$]$_3$TAPB-PA	N(1)-H(1W)···O(8)	1.01	1.72	2.724(3)	171
	N(1)-H(1W)···O(9)	1.01	2.61	3.149(3)	113
	N(2)-H(2W)···O(15)	1.04	1.71	2.719(3)	161
	N(2)-H(2W)···O(21)	1.04	2.41	3.027(3)	117
	N(3)-H(3W)···O(1)	1.00	1.71	2.697(3)	167
	C(2)-H(2)···O(4)	0.95	2.49	3.428(4)	171
	C(11)-H(11)···O(19)	0.95	2.36	3.234(4)	152
	C(13)-H(13A)···O(9)	0.98	2.52	3.220(4)	128
	C(13)-H(13B)···O(13)	0.98	2.53	3.313(4)	137
	C(13)-H(13C)···O(8)	0.98	2.48	3.400(4)	156
	C(14)-H(14A)···O(20)	0.98	2.58	3.405(5)	149
	C(14)-H(14A)···O(9)	0.98	2.44	3.143(5)	128
	C(17)-H(17)···O(15)	0.95	2.26	3.026(4)	137
	C(21)-H(21A)···O(21)	0.98	2.44	3.070(4)	122
	C(22)-H(22B)···O(3)	0.98	2.37	3.129(4)	134
	C(25)-H(25)···O(10)	0.95	2.40	3.334(4)	166
	C(27)-H(27)···O(1)	0.95	2.51	3.219(4)	131
	C(29)-H(29A)···O(2)	0.98	2.51	3.413(4)	123
	C(30)-H(30A)···O(2)	0.98	2.34	3.020(4)	126
	C(30)-H(30B)···O(7)	0.98	2.43	3.311(4)	128
	C(30)-H(30B)···O(13)	0.98	2.38	3.217(4)	144

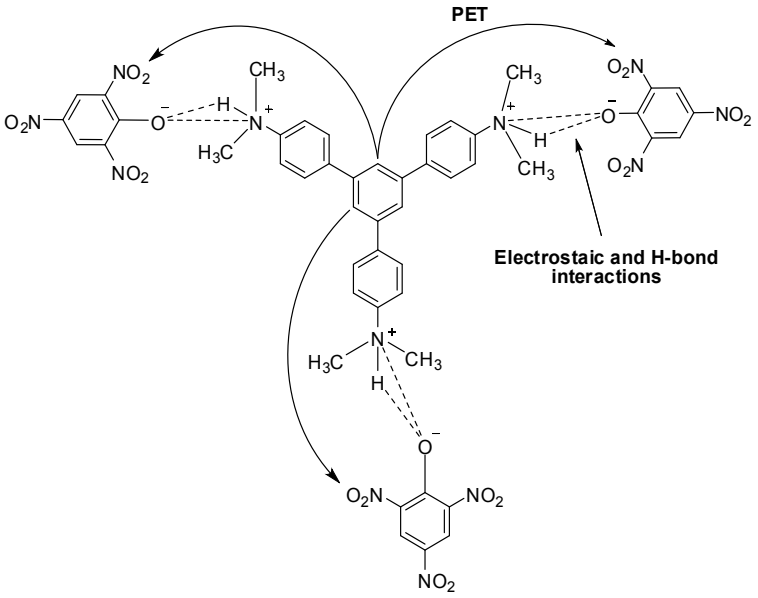

Fig S15. Mechanism of electrostatic and H-bonds induced PET process in the fluorophore [(*N*,*N*)Me_2]$_3$TAPB with PA.

Calculation of detection limit. To determine detection limit (DL), fluorescence titration of compound [(*N*,*N*)Me_2]$_3$TAPB (1.0 μM) with PA has been carried out. The successive fluorescence intensities have been plotted as a function of concentration of to obtain the correlation curve which shows linear ralationship with the [PA] in the range of 1.0 to 4.0 μM. Standard deviation for blank solution (Sb1), slope of the curve (S) and signal to noise ratio (K) = 3 have been calculated from the curve and substituted in the following equation to calculate DL.

$$\mathrm{DL} = \mathrm{K} \times \frac{Sb1}{S}$$

Results of the analysis are as follows:

Sb1 = 278.090, S = 123.3428 × 10^6 and DL = 6.76 × 10^{-6} M or 1.50 ppm.

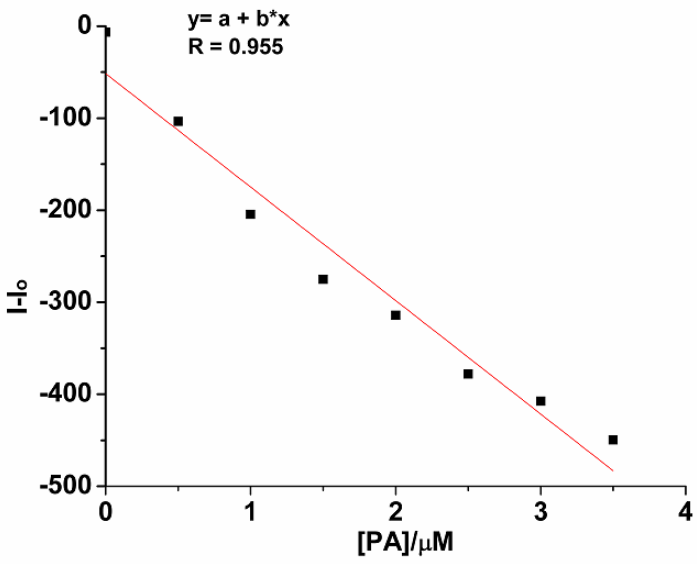

Fig S16. Linear correlation curve for the calculation of DL (fluorescence intensity at 427 nm versus concentration).

References;

(1) G. He, H. Peng, T. Liu, M. Yang, Y. Zhang and Y. Fang, *J. Mater. Chem*., 2009, **19**, 7347-7353.

(2) D. Li, J. Liu, R. T. K. Kwok, Z. Liang, B. Z. Tang and J. Yu, *Chem. Commun.*, 2012, **48**, 7167-7169.

(3) M. Wang, V. Vajpayee, S. Shanmugaraju, Y.-R. Zheng, Z. Zhao, H. Kim, P. S. Mukherjee, K.-W. Chi and P. J. Stang, *Inorg. Chem.*, 2011, **50**, 1506-1512.

(4) P. Lu, J. W. Y. Lam, J. Liu, C. K. W. Jim, W. Yuan, N. Xie, Y. Zhong, Q. Hu, K. S. Wong, K. K. L. Cheukand B. Z. Tang, *Macromol. Rapid Commun.*, 2010, **31**, 834-839.

(5) T. Liu, L. Ding, G. He, Y. Yang, W. Wang and Y. Fang, *ACS Appl. Mater. Interfaces*, 2011, **3**, 1245-1253.

(6) V. Bhalla, A. Guptaand M. Kumar, *Org. Lett.*, 2012, **14**, 3112-3115.

(7) N. Dey, S. K. Samantaand S. Bhattacharya, *ACS Appl. Mater. Interfaces*, 2013, **5**, 8394-8400.

(8) N. Venkatramaiah, S. Kumarand S. Patil, *Chem. Commun.*, 2012, **48**, 5007-5009.

(9) H.-T. Feng and Y.-S. Zheng, *Chem. Eur. J.*, 2013, **20**, 195-201.

(10) X. Wang, Y. Guo, D. Li and H. Chenand R.-c. Sun, *Chem. Commun.*, 2012, **48**, 5569-5571.

(11) V. Vij, V. Bhalla, and M. Kumar, *ACS Appl. Mater. Interfaces*, 2013, **5**, 5373-5380.

(12) M. Dong, Y.-W. Wang, A.-J. Zhang and Y. Peng *Chem. Asian J.* 2013, **8**, 1321-1330.

(13) S. Dalapati, S. Jin, J. Gao, Y. Xu, A. Nagai and D. Jiang, *J. Am. Chem. Soc.* 2013, **135**, 17310-17313.

(14) V. Bhalla; S. Kaur, V. Vij and M. Kumar *Inorg. Chem.* 2013, **52**, 4860-4865.

(15) P. Vishnoi, M. G. Walawalkar, S. Sen, A. Datta, G. N. Patwari and R. Murugavel, *Phys. Chem. Chem. Phys.* 2014, **16**, 10651-10658.